Ultrasonics 92 (2019) 13–20

Contents lists available at ScienceDirect

Ultrasonics

journal homepage: www.elsevier.com/locate/ultras

Lamb waves and electro-mechanical impedance based damage detection using a mobile PZT transducer set

Yuebin Zheng, Kehai Liu, Zhanjun Wu*, Dongyue Gao, Rahim Gorgin, Shuyi Ma, Zhenkun Lei

State Key Laboratory of Structural Analysis for Industrial Equipment, Dalian University of Technology, Dalian 116024, China

ARTICLE INFO

Keywords:
Lamb waves
Electro-mechanical impedance
Damage detection
mobile PZT transducer
Baseline-free

ABSTRACT

Lamb waves and electro-mechanical impedance (EMI) based methods are increasingly used in damage detection owing to their high sensitivity to small structural defects. Lamb wave based methods are effective in detecting damages in a large area and electro-impedance based methods are suitable for characterizing the identified damage. Based on these two methods, a novel combined damage detection method is presented in this research. To achieve this, first, a mobile transducer set is developed, which can be used for both the Lamb waves and EMI based methods. Then, a baseline-free damage detection strategy that combines the Lamb waves and EMI methods is presented. Finally, a laboratory-sized test piece is used to validate the effectiveness of the proposed approach. The results achieved with the application of the presented combined method for characterizing an L-shape crack in an aluminum plate show better location accuracy and detection efficiency than those obtained by applying only one method.

1. Introduction

Engineering structures, such as those in aircraft, civil infrastructure, and heavy equipment, usually suffer adverse serving conditions or even sudden impacts, which may easily cause structural defects. Thus, damage detection techniques have always been a major industrial concern in the fields of non-destructive evaluation (NDE) and structural health monitoring (SHM). The most common NDE and SHM techniques include visual inspection, optical fibers, shearography, infrared thermography, eddy currents, ultrasonic inspection, Lamb waves, and electromechanical impedance (EMI). Among the damage detection methods, the Lamb wave based and EMI methods are being increasingly used in recent years for their high sensitivity to structural damage [1–5].

In the EMI-based method, the electrical impedance of the piezoelectric lead zirconate titanate (PZTs) can be directly related to the mechanical impedance of the host structure by the coupling between the sensor and the structure [6]. Hence, if the mechanical impedance of the host structure varies because of damage, the measured EMI signals will also be affected [7]. The EMI method is suitable for local damage detection owing to its sensitivity to the presence and propagation of damage [8]. Lately, some valuable studies have been conducted, including quantitative damage detection in pipelines using multiple EMI sensors [9], quantification of corrosion damage using an innovative mechanical impedance-based technique on steel structures [10], and differentiation between two types of damages using time–frequency analysis of EMI [11]. However, although the EMI method can be highly sensitive to even a small damage under high-frequency ranges, the sensing area of the PZT was extremely small and the method could not detect damage in the far field [12].

In comparison with the EMI method, Lamb waves can achieve a larger sensing area and be faster and more cost-effective to locate damage [13,14]. Lamb waves based damage detection methods utilize a specific type of ultrasonic guided waves that remain guided between two parallel free surfaces, such as the top and bottom surfaces of a plate or of shell like structures. Lamb waves can be generated and received by various kinds of transducers including ultrasonic probes [15], laser-based ultrasonics [16], electromagnetic acoustic transducers (EMAT) [17–19], PZT wafer/elements [13,20], interdigital transducers using polyvinylidene fluoride (PVDF) [21] (mainly used as a sensor), and fiber Bragg grating (FBG) [22] (only used as a sensor). Structural damages can be identified by extracting and evaluating the changes in Lamb waves characteristics, such as reflections, scattering, and mode conversion, owing to the interaction between waves and damage [13,23]. However, such changes are usually defined by comparing the current signal with a baseline signal [24–26], and they can be easily affected by environmental and operational changes [27–30]. Moreover, it is difficult to analyze and interpret Lamb wave signals owing to the

* Corresponding author.
E-mail address: wuzhj@dlut.edu.cn (Z. Wu).

https://doi.org/10.1016/j.ultras.2018.06.008
Received 7 February 2018; Received in revised form 27 May 2018; Accepted 11 June 2018
Available online 13 June 2018
0041-624X/

dispersion and multi-modal properties in wave propagation; therefore, to a certain degree, the application of Lamb waves is less concise and accurate for characterizing damage [31].

The combination of the Lamb wave and EMI methods retains the advantages of both. This procedure is capable of global damage detection using Lamb waves and of localized damage characterization by measuring impedance [32–34]. Therefore, the same PZT patches can be used for both methods and the structural area can be covered completely [32,33]. Besides, an integrated system that drives the same PZTs by changing the detection mode could have less complexity to a certain degree. Recently, some useful attempts have been done to capture the benefits of these two methods [31,35,36]. However, these works all depend on the baseline data. Besides, sensors must be pre-arranged at critical structural locations for EMI measurement. A mature scheme offering increased accuracy and higher efficiency is still in exploration. The development of mobile robot systems for damage detection is a trend for the future. To make them more efficient and intelligent, a suitable detection strategy is necessary.

In this study, a novel combined damage-detection strategy based on the Lamb waves and EMI methods using a mobile transducer set is developed. Firstly, the proposed strategy does not need a baseline signal. For the Lamb waves, a baseline-free probability-based damage imaging technique is employed to identify the healthy and damaged areas quickly. The measured EMI signals in the healthy area could then be examined and calculated as “reference data”, instead of any previously obtained baseline data. In this way, the proposed strategy minimizes false detections caused by non-damage related variations in both methods. Secondly, in order to generate and collect signals, a mobile transducer set containing PZT patches is developed. The initial design idea of the mobile transducer set is based on a previous work [37]. In the future, mobile robots equipped with the transducer set for damage detection will be taken into consideration. Compared to the traditional PZT patches, which are permanently attached to the structure, the mobile transducer set can be easily attached and removed from the surface of the structure. Thus, the mobile transducer can flexibly move to any region of interest in the structure. Finally, an algorithm to construct an impedance image based on the EMI method is developed. The algorithm includes an outlier analysis and the probability image can improve the final detection result with higher accuracy than the previous results based on Lamb waves.

The remainder of this article is divided into three sections. In Section 2, the combined damage detection strategy is presented. In Section 3, first, the design of the mobile transducer set is reviewed, and then experimental studies are conducted to validate the effectiveness of the proposed approach. In the last section, conclusions with a brief summary are given.

2. Methodology

2.1. Approach

A novel combined damage-detection approach based on the Lamb waves and EMI methods is developed. For that purpose, a mobile transducer is utilized to generate and collect signals on the surface of a test specimen. The overall procedure of the proposed approach is illustrated in Fig. 1.

Firstly, using Lamb waves, a baseline-free probability-based damage imaging (PDI) technique is employed to identify the healthy and damaged areas quickly. Here, this procedure can be called as global damage detection. Secondly, the impedance signals of the mobile transducer are measured in both the healthy and damaged areas. Then, the impedance signals of both areas are used to improve the final damage diagnostic image. The second procedure can be called as local damage detection. In the final outcome, the proposed approach is capable of locating damage in a large-scale structure quickly, and also of improving the accuracy of identifying the most probable location of the damage in the local damaged area.

Fig. 2 illustrates the specific process of the proposed approach. The first procedure, called global damage detection, is based on the previous work performed by Rahim Gorgin et al. [38]. First, a relatively pure A_0 mode is generated and the corresponding signal at different locations of the structure is collected using mobile PZT transducers. Subsequently, a damage scatter signal is defined via a signal separation process without relying on any previous baseline data. Then, the amplitude of the energy envelope of the damage scatter signal is considered as the damage presence probability index (DPPI) to construct the damage diagnostic image. The diagnostic image highlights the most probable locations of damages in the whole detection area. At last, by adjusting the diagnostic image threshold, the local damaged and healthy areas are confirmed. In general, the threshold should be determined by the location of the peak of the diagnostic image and the half-distance between two locations of detection. Thus, the damage could be located within the local damaged area.

The second procedure, called local damage detection, uses the EMI method with the same mobile PZT transducer set. In this procedure, firstly, the impedance signals of the mobile transducer are measured in both the healthy and local damaged areas. Subsequently, the average value of all the impedance signals measured in the healthy area is calculated as the average impedance data of the intact structure, instead of using previous baseline data. Then, the changes in the impedance signals owing to damage in the local damaged area are calculated through root-mean-square deviation (RMSD) as damage indices to construct the damage diagnostic image. Furthermore, an outlier analysis is conducted to define the threshold value regarding the impedance signals in the local damaged area.

2.2. Lamb wave based damage location identification for global detection

2.2.1. Damage scatter separating process

By placing the mobile PZT sensor very close to the actuator, the signal separation process can be applied to define the damage scatter signal [30]. As the distance between the actuator and the sensor is very short, the wave coming directly from the actuator travels for only a very short time and so, appears almost at the very beginning of the received signal. By calculating the travel time between the sensor and the actuator, because the distance L_{as} and speed of the selected Lamb wave mode V_L are known, this wave can be separated from the damage scatter and boundary reflections. Similarly, according to the location of the transducer set on the test piece and speed of the selected Lamb wave mode V_L, the time at which the first boundary reflections will appear in the received signal can also be calculated. Therefore, when the signal is multiplied by a time window function, only the damage scatter wave will be preserved. The time window function is expressed as follows:

$$f = \begin{cases} 0 & 0 \leqslant t < t_1 \\ 1 & t_1 \leqslant t < t_2,\ t_1 = \dfrac{L_{as}}{V_L} + L_s,\ t_2 = t_1 + \dfrac{2L_{asb}}{V_L}, \\ 0 & t \geqslant t_2 \end{cases} \tag{1}$$

where t_1 denotes the end time of the wave coming directly from the actuator; t_2 denotes the beginning time of the boundary reflections; L_{as}, L_s, and L_{asb} denote the distance between the sensor and actuator, length of the excitation signal, and distance between the transducer set to the nearest structure boundary, respectively; and V_L denotes the velocity of the selected Lamb wave mode.

2.2.2. Damage diagnostic imaging

The amplitude of the energy envelope of the scatter signal can be considered as the damage presence probability index (DPPI). Then, a diagnostic image can be constructed by relating the contrast at a particular pixel to its corresponding DPPI value. A Hilbert transform of the scatter signals was defined for this purpose. For an arbitrary signal $f(t)$, the Hilbert transform is defined as follows [39]:

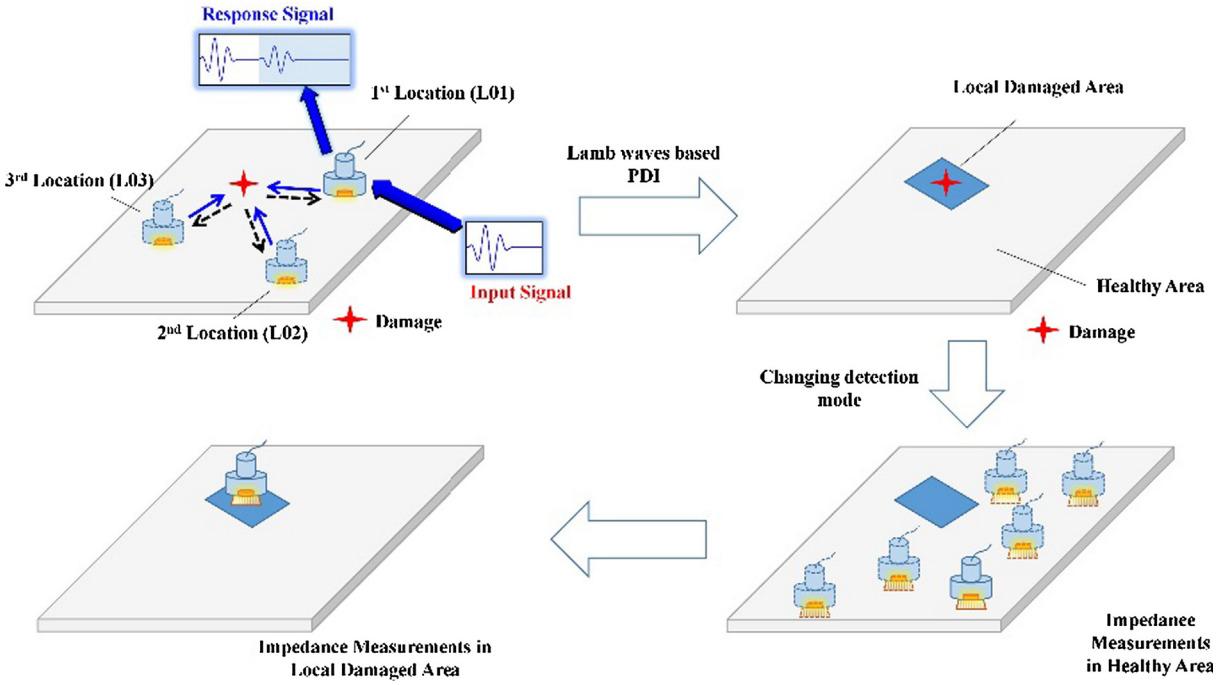

Fig. 1. Overall procedure of the proposed approach.

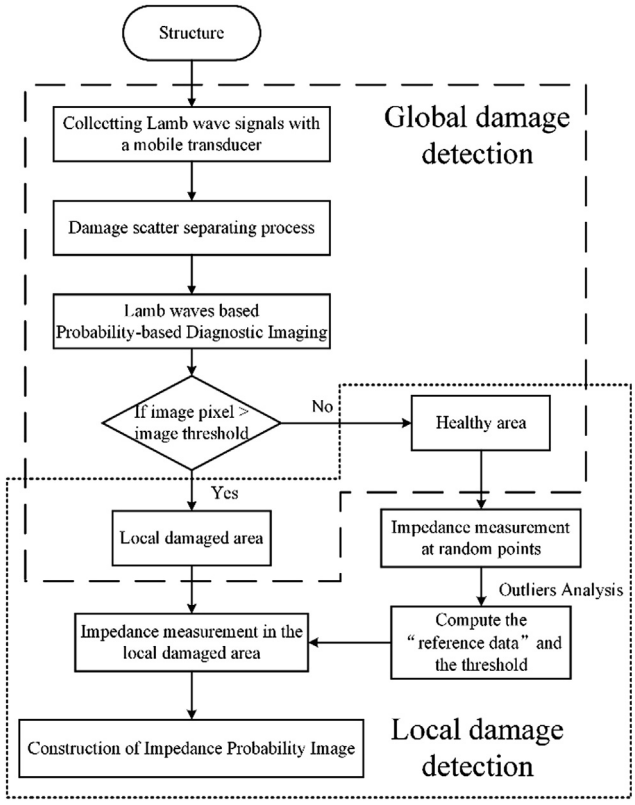

Fig. 2. Specific process of the proposed approach.

$$H(t) = \frac{1}{\pi}\int_{-\infty}^{+\infty}\frac{f(t')}{t-t'}dt'. \tag{2}$$

This equation performs a 90° phase shift to construct an analytic signal $F_A(t)$

$$F_A(t) = f(t) + iH(t) = e(t), \tag{3}$$

where $e(t) = \sqrt{f^2(t) + H^2(t)}$ and $\phi(t) = \arctan\frac{H(t)}{f(t)}$. The real part of the analytic signal is the original signal $f(t)$ itself and its imaginary part is the corresponding Hilbert transform $H(t)$. $e(t)$ is the module of $F_A(t)$ and $\phi(t)$ is the instantaneous phase. Thus, the envelop of $e(t)$ depicts the energy distribution of the original signal in the time domain.

After the energy envelope of the damage scatter signals has been obtained, the probability of damage presence at all nodes with regard to all damage scatter signals can be defined as follows [2]{Zhou, 2011 #383}:

$$\begin{cases} p(i,j) = \sum_m^N w_m e_m(t_{mij}) \\ t_{mij} = \frac{L_m^{ad} + L_m^{ds}}{V} \end{cases}, m = 1, 2, ...,N, \tag{4}$$

where $p(i,j)$ is the probability of damage presence at the imaging pixel (i,j), $e_m(t)$ denotes the energy envelope of scatter signals acquired at location m, t_{mij} is the time that corresponds to the wave travel from the actuator to the imaging pixel (i,j) and then to the sensor, L_m^{ad} and L_m^{as} denote the distances between the actuator located at location m to the imaging pixel (i,j) and from the imaging pixel (i,j) to the sensor located at location m, respectively. The parameter V denotes the speed of the Lamb wave, which may vary significantly with the center frequency. The parameter w_m refers to the appropriate weight that compensates the performance difference among the different responses, and which in the simplest case would be equal to unity for uniform weighting.

The imaging pixels with the highest probability of damage presence highlight the most probable locations of damage in the monitoring area.

2.3. EMI-based damage characterization for local detection

2.3.1. Conventional EMI method

An electro-mechanical system consisting of a PZT and a host structure can be modeled as a single degree-of-freedom (SDOF) spring-mass-damper system [6]. Then, the admittance signal $Y(\omega)$, which is the inverse of the impedance $Z(\omega)$, can be expressed as

$$Y(\omega) = \frac{1}{Z(\omega)} = i\omega\frac{w_A l_A}{h_A}\left(\bar{\varepsilon}_{33}^E - d_{31}^2\bar{Y}_{11}^E + \frac{Z_A d_{31}^2 \bar{Y}_{11}^E}{Z_A + Z_s}\frac{\tan(kl_A)}{kl_A}\right), \tag{5}$$

where l_A, w_A, and h_A indicate the length, width, and thickness of the

PZT, respectively. d_{31}^2 is the piezoelectric strain coefficient and $\bar{\varepsilon}_{33}^E = (1-\delta j)\varepsilon_{33}^E$ is the complex electric permittivity of the PZT material at constant stress. $\bar{Y}_{11}^E = (1-\eta j)Y_{11}^E$ is the complex Young's modulus of the PZT material at a constant electric field. δ and η denote, respectively, the dielectric loss factor and mechanical loss factor of the PZT. The parameters ω, k, Z_A, and Z_s represent the angular frequency, wave number, mechanical impedance of the PZT, and short-circuited mechanical impedance of the host structure, respectively.

In the conventional EMI method, simple statistical algorithms, which are based on frequency-by-frequency comparisons, can be chosen as the scalar damage metrics. One of the commonly used is the RMSD [7]:

$$RMSD = \sum_{i=0}^{N} \sqrt{(Re(Z_i) - Re(Z_i^0))^2 / Re(Z_i^0)^2}, \tag{6}$$

where RMSD denotes the damage metric, $Re(Z_i^0)$ is the real part of the PZT measured impedance at the last condition, and $Re(Z_i)$ is the real part of the measured impedance at the current condition. Generally, the greater the value of RMSD, the larger the difference between the two conditions is, which indicates the presence of damage in the structure. In most cases, the metric values increase when there is an increase in the severity of damage. For each impedance sensor, the sensing range is closely related to the material and geometric properties of the host structure, frequency ranges being selected, and material properties of the PZT [32]. Under the high-frequency ranges, the sensing region is limited to an area close to the PZT sensor/actuator. Thus, the traditional EMI method reflects the localized state of a structure.

2.3.2. Construction of impedance probability image

In the healthy area, the average value of the measured impedance signal was collected by successively placing the mobile PZT transducer set at different random locations. The average impedance data can be regarded as the reference data in the RMSD calculation. Thus, the reference does not rely on any previous baseline data but, instead, on the average impedance data. Then, through RMSD, the statistical differences between the impedance data at a random location and the average impedance data should be calculated as the random error distribution, which can be expressed as follows:

$$X^m = RMSD(Re(Z_i)^m) = \sum_{i=0}^{N} \sqrt{(Re(Z_i)^m - Re(Z_i^0))^2 / Re(Z_i^0)^2}, \tag{7}$$

where $Re(Z_i^0)$ is the average impedance data and $Re(Z_i)^m$ is the impedance data at location $m (m = 1, 2, ..., M)$; then, X^m represents the random error value of the impedance at location m and N is the number of data points.

Subsequently, an outlier analysis is applied to define the threshold value that indicates the presence of structural damage. If there are outliers in a series of independent and equal precision data $x_1, x_2, ..., x_m$ and the data set is not very large, the Romannovschi criterion can be applied to identify outliers that are regarded as related to the structure defects [40]. If x_j is the largest data, then

$$\bar{x}(j) = \frac{1}{m-1} \sum_{i \neq j} x_i, \tag{8}$$

$$v_i = x_i - \bar{x}(j), \ 1 \leqslant i \leqslant m, \tag{9}$$

$$\sigma^2(j) = \frac{1}{m-2} \sum_{i \neq j} v_i^2. \tag{10}$$

Therefore, if

$$|x_j - \bar{x}(j)| > K(m, a)\sigma(j), \tag{11}$$

x_j is an outlier; otherwise, x_j is a normal data point.

After eliminating the outliers, the threshold value (TR) can be calculated as follows:

$$TR = \mu + K(m, a)\sigma, \tag{12}$$

Table 1
Values of $K(m, a)$.

$m \backslash a$	0.05	0.01	$m \backslash a$	0.05	0.01
4	4.97	11.45	17	2.20	3.04
5	3.56	6.53	18	2.18	3.01
6	3.04	5.04	19	2.17	3.00
7	2.78	4.36	20	2.16	2.95
8	2.62	3.96	21	2.15	2.93
9	2.51	3.71	22	2.14	2.91
10	2.43	3.54	23	2.13	2.90
11	2.37	3.41	24	2.12	2.88
12	2.33	3.31	25	2.11	2.86
13	2.29	3.23	26	2.10	2.85
14	2.26	3.17	27	2.10	2.84
15	2.24	3.12	28	2.09	2.83
16	2.22	3.08	29	2.09	2.82

where TR represents the threshold value for RMSD, a is the level of significance, and μ and σ are the mean and standard deviation for the random error distribution X^m, respectively. For m from 4 to 29 and a of 0.05 and 0.01, $K(m, a)$ values are listed in Table 1 [40].

If the data set is large (in general, $n \geqslant 20$), the Grubbs criterion can be applied instead of the Romannovschi criterion. More details can be seen in Ref. [40].

According to Ref. [34], the damage metric tends to decrease linearly as the crack moves away from the sensor. Thus, in this study, the detection area of the transducer set is assumed as a circular area and the location of the transducer set is considered to be at the center of the circle. The detection radius of the EMI-based method is assumed as r; thus, the local damaged area can be partitioned into many full circular areas of the same size with detection radius r(the areas can overlap). The detection radius r should be determined by the structure and swept frequency in the impedance measurements. In general, the detection radius r is approximately twice or three times the radius of the transducer. The centers of such circular areas are recorded as location $n (i = 1, 2, ..., N)$. As the mobile transducer set can move easily on the structure, it can be placed at location n so that the impedance signals of the transducer set could be measured. Therefore, the RMSD index could be calculated as X^n in Eq. (7) at location n. The damage presence probability of the image $I_n(i, j)$ at each pixel (i, j) can then be defined as follows:

$$I_n(i, j) = X^n W(d_{nij}), \tag{13}$$

where d_{nij} represents the distance between the pixel (i, j) and the location n and $W(d_{nij})$ means that only the pixel (i, j) contained in the detection area can be used to construct the diagnostic image. d_{nij} and $W(d_{nij})$ can be defined as follows, respectively:

$$W(d_{nij}) = \begin{cases} 1 - \frac{d_{nij}}{r} \text{ when } d_{nij} \leqslant r \\ 0 \text{ when } d_{nij} > r \end{cases}, \tag{14}$$

$$d_{nij} = \sqrt{(x_n - x_i)^2 + (y_n - y_j)^2}. \tag{15}$$

The diagnostic image can then be constructed by taking a summation of all the I_n defined at different locations

$$P(x, y) = \sum_{n=1}^{N} I_n(i, j), \tag{16}$$

where $P(x, y)$ is the probability of damage presence in the imaging pixel (i, j). The pixels with maximum field values highlight the most probable locations of the damages in the detection area.

3. Experimental study

In this research, a mobile transducer set that contains a PZT is developed to combine the Lamb wave and EMI methods, which can

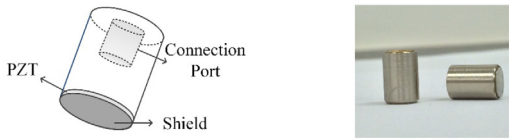

(a) Schematic of the transducer set (b) Picture of the transducer set

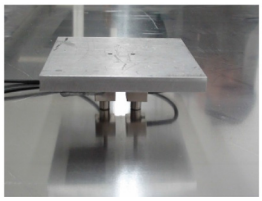

(c) Assembly of the mobile transducer set

Fig. 3. The designed mobile transducer.

improve the practicability and performance of damage detection methods. The mobile transducer consists of the PZT element, damping medium, shield, and connection port. The PZT element is used to excite/receive Lamb waves and characterize EMI signals. A damping medium is attached to the top of the PZT element to increase its flexural rigidity. The shield is attached to the bottom of the PZT to cover the PZT element and prevent it from friction and damage. The positive and negative poles of the PZT element are connected with the connection port, and finally, all the components are assembled into the transducer device. The designed mobile transducer is shown in Fig. 3. The mobile PZT transducer set is firmly pressed down to the surface of the structure. A coupled force is applied by a constant vertical load. In this way, the energy between the PZT transducer and the structure is transmitted by dry contact. A series of tests were performed to determine the effect of the coupled force on the response of the transducer. These results indicate that a coupled force of nearly 30 N is sufficient for stable coupling.

In this section, an experimental study is performed to investigate the feasibility of the presented damage detection method. Lamb waves were first used for detecting and locating through-thickness cracks in an aluminum plate quickly. After confirming the local damaged area, the impedance-based method was then used to characterize the crack damage more precisely in the improved diagnostic image.

All the tests were carried on an aluminum plate (1000 mm × 1000 mm × 3 mm), which was fixed along its four edges on a testing table. An L-shape crack was introduced into the plate, as seen in Fig. 4.

3.1. Lamb waves based global damage detection procedure in aluminum plate

3.1.1. Experimental setup

In the first procedure, a kind of grease lubricant is placed under the bottom surface of the sensor and actuator. In this way, a strong vertical pressure will be generated by the actuator to the plate to excite theA_0 mode and decrease the shear force between the actuator and the plate to weaken S_0 mode. To this end, a comparatively pure A_0 mode can be excited. A 5-cycle sinusoidal tone burst enclosed in a Hanning window at a central frequency of 50 kHz was generated by an arbitrary waveform generation (Agilent 33220A). The length of the excitation signal L was easily calculated as 0.17 ms. The wave signals were collected by an oscilloscope (Agilent DSO5032A) with sampling rate of 10 MHz. The sampled signals were transmitted into the central processing unit for further processing and analysis. The A_0 mode velocity is assumed as constant in this study. The straight distance between the center of the sensor and the actuator is 2 cm. Lamb waves are generated and the corresponding responses at different locations on the plate (L1, L2, …, L25, shown in Fig. 4) are collected. The signal acquisition positions are listed in Table 2.

3.1.2. Results and discussion

All the responses were normalized. Typical damage scatter signals at locations L9 and L18 are shown in Fig. 4. Then, the diagnostic image could be constructed using equation and displayed as a contour map, as shown in Fig. 5. In Fig. 5, the area encircled by the contour line 0.8 represents the highest probability of damage presence. The damaged area indicates the probable location of damage, although in this procedure the shape and size of the L-shape crack cannot be recognized yet. The shortest distance between the location of the peak of the diagnostic image (whose coordinate is (0.66, 0.16), unit: m, and is marked by the red '×') and the damage is 4.5 cm.

Thus, the local damaged and healthy areas are confirmed by adjusting the image threshold to 0.8. The area (circled by a black dotted line) located the L-shape crack (marked by a dark line), and thus, it was chosen as the local damaged area, as seen in Fig. 5. The area of this local damaged area is calculated as 100 mm × 150 mm, which is determined by the half-distance between the two locations of detection.

3.2. EMI-based local damage detection procedure in aluminum plate

3.2.1. Experimental setup

Impedance measurements were carried out by a commercial impedance analyzer (Wayne Kerr 6500B). The maximum speed was set for the measurement function. A frequency range between 50 kHz and 500 kHz was determined by the trial and error method [32]. As there is a relatively high mode density within this range, it generally covers more structural dynamic information [32].

After confirming the local damaged area, the procedure continues with the second part. The local damaged area was partitioned into many full circular areas of the same size with detection radius r. The centers of such circular areas were recorded as location $n(i = 1, 2, ...,N)$. The mobile transducer set was placed at location n and 10 random locations in the healthy area, and then the impedance signals were measured at these locations. In this study, the detection radius r was selected as 30 mm. Further, based on the area of the local damaged area (100 mm × 150 mm), the total number N of EMI measurement locations was $4 \times 5 = 20$.

3.2.2. Results and discussion

The measured impedance signals at 10 random locations (p1–p10) in the healthy area are shown in Fig. 6. The RMSD indices $\{X^1, X^2, ...,X^{10}\}$ of these 10 locations are listed in Table 3, and the 3-D histogram is shown in Fig. 7.

As mentioned above, the energy between the mobile transducer and the structure is transmitted by dry contact, and thus, the outlier analysis was employed firstly to ensure the stability of the impedance signals. As the data set $\{X^1, X^2, ...,X^{10}\}$ was not large (less than 20), Romannovschi criterion was selected to detect abnormal data. Therefore, there are no outliers in the data set $\{X^1, X^2, ...,X^{10}\}$; thus, all the impedance signals of the random locations in the healthy area were sufficiently stable. Using Eqs. (11) and (12), the TR was 0.7594 ($a = 0.01$, $m = 10$). The mean value and the threshold (TR) of the data set $\{X^1, X^2, ...,X^{10}\}$ is shown in Fig. 8.

Subsequently, the average value of all the impedance signals measured in the healthy area is calculated as the average impedance data. The measured impedance signals at typical locations in the local damaged area are shown in Fig. 9. As seen in Fig. 9, when the mobile transducer was placed far away from the crack the impedance signal did not significantly changed compared to the average impedance data, while the RMSD index of this location was 0.4631, which is lower than the TR. When the mobile transducer was placed at the edge of the crack, the impedance signal changed compared to the average impedance data. Moreover, the RMSD index at this location was 2.2353, higher than the TR, which indicates the presence of structural damage. When

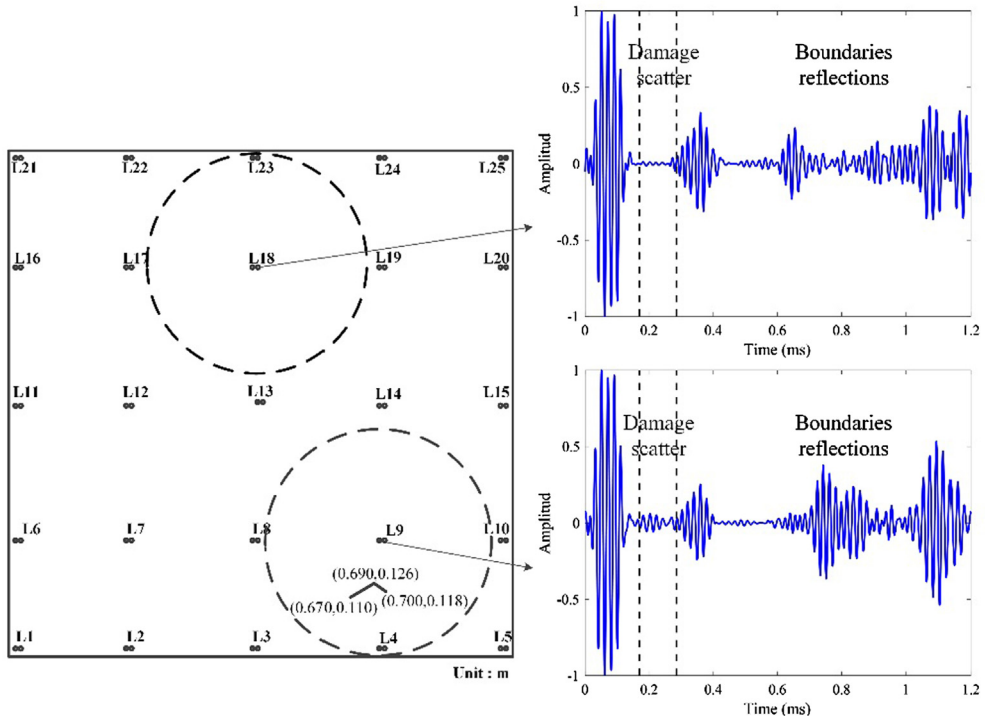

Fig. 4. Experimental Setup and typical responses collected by the transducer set at locations L9, L18.

Table 2
Coordinates of signal acquisition locations on test plate.

Position	Coordinates (x, y)/(m)	Position	Coordinates (x, y)/(m)
L01	(0.015, 0.005)	L14	(0.700, 0.500)
L02	(0.300, 0.005)	L15	(0.985, 0.500)
L03	(0.500, 0.005)	L16	(0.015, 0.700)
L04	(0.700, 0.005)	L17	(0.300, 0.700)
L05	(0.985, 0.005)	L18	(0.500, 0.700)
L06	(0.015, 0.300)	L19	(0.700, 0.700)
L07	(0.300, 0.300)	L20	(0.985, 0.700)
L08	(0.500, 0.300)	L21	(0.015, 0.995)
L09	(0.700, 0.300)	L22	(0.300, 0.995)
L10	(0.985, 0.300)	L23	(0.500, 0.995)
L11	(0.015, 0.500)	L24	(0.700, 0.995)
L12	(0.300, 0.500)	L25	(0.985, 0.995)
L13	(0.500, 0.500)		

the mobile transducer was placed at the crack, the impedance signal substantially changed compared to the average impedance data, and the RMSD index at this location was 4.3316. The result shows that the impedance signals of the mobile transducer are sensitive to small structural damages.

Then, using Eqs. (13)–(16), the RMSDs in the local damaged area are calculated as damage indices to construct the damage diagnostic image. It is displayed as a contour map, as shown in Fig. 10.

In Fig. 10, the region of the contour map where the contour value is higher than a certain threshold may be assumed to represent the shape and size of the damage. To this end, presenting the identification results in terms of the probability of damage, based on the fusion of signals rendered by a number of impedance signals at different locations, is an advantage over the traditionally performed EMI method, as described in Section 2.3.1.

The location of the actual crack is marked as a dark line. According to Fig. 10, the region with the highest probability of damage presence coincided relatively well with the actual damage. The shortest distance between the location of the peak of the diagnostic image (the coordinate is (0.69, 0.13), unit: m, and is marked by the blue '×') and the damage is 0.04 cm. The final result improves the accuracy of the most probable location of damage, compared to the Lamb wave result in Fig. 5.

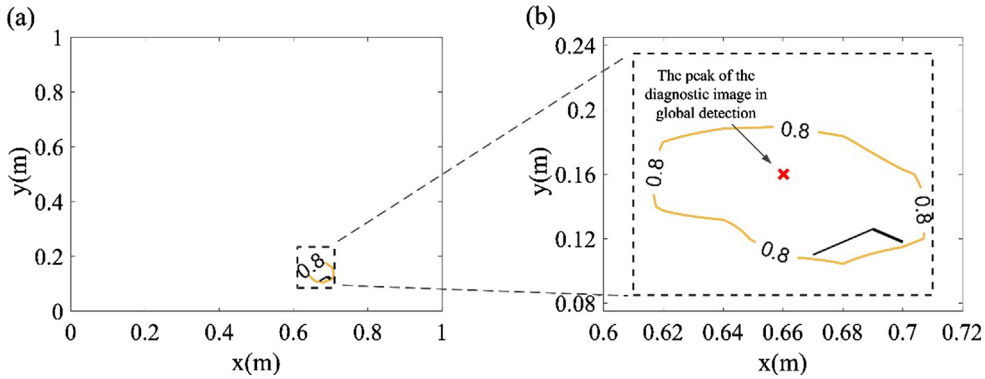

Fig. 5. Result of Lamb waves based global detection: (a) contour map in the whole detection area, (b) zoom in to the local damaged area. The peak of the image is marked by the red '×' and the L-shape crack is marked by the dark line.

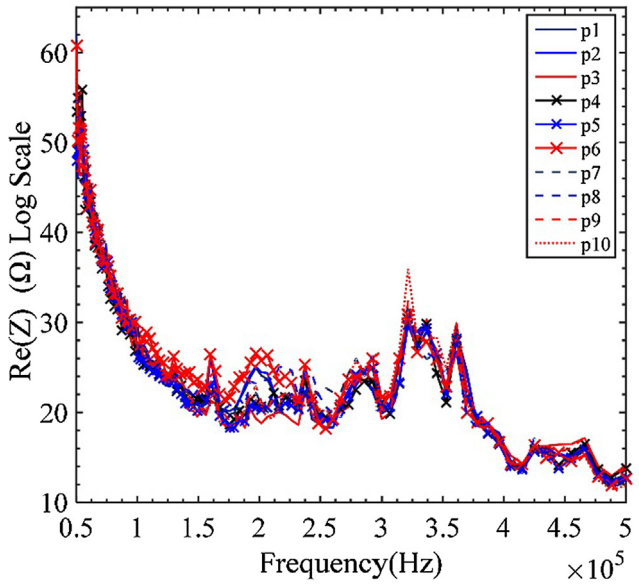

Fig. 6. Measured impedance signals at 10 random locations (p1–p10) in the healthy area.

Table 3
RMSD of the data set $\{X^1, X^2, ..., X^{10}\}$

Location	RMSD	Location	RMSD
p1	0.4458	p6	0.6337
p2	0.4265	p7	0.4662
p3	0.6278	p8	0.5271
p4	0.4718	p9	0.4151
p5	0.4474	p10	0.5045

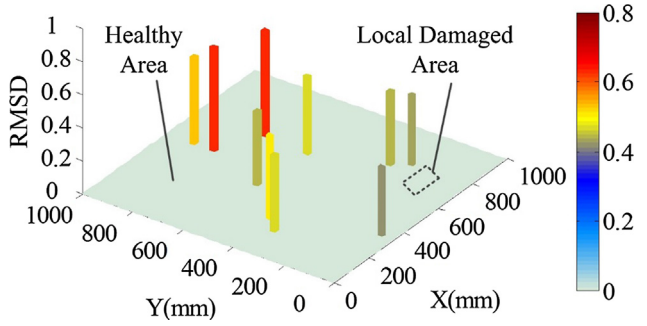

Fig. 7. RMSD at 10 random locations (p1–p10) in the healthy area.

Furthermore, independently of the Lamb wave or EMI method, most of the time necessary for each measurement is spent in moving and placing the transducer set, and it can be estimated at 10 s in this research. Then, the time required for the combined detection can be calculated as (25 + 20 + 10) × 10 = 550 s. Compared to the area of the whole structure (1000 mm × 1000 mm), the area of the local damaged area (100 mm × 150 mm) was narrowed down to 0.015. If the local damaged area had not been determined by Lamb waves first, the time consumption for the EMI measurement of the whole structure would have been of approximately 20 × 10/0.015 ≈ 13333 s. It is obvious that the proposed combined approach can improve the detection efficiency in comparison with the EMI method.

4. Conclusion

This article proposed a novel damage-detection approach combining the Lamb waves and EMI methods with the use of a mobile PZT transducer set. This combined approach retains the advantages of these two methods, such as the capability to locate damage in a large-scale structure quickly and to improve the accuracy of the most probable location of damage in the local damaged area. Moreover, it can detect damage without relying on baseline data.

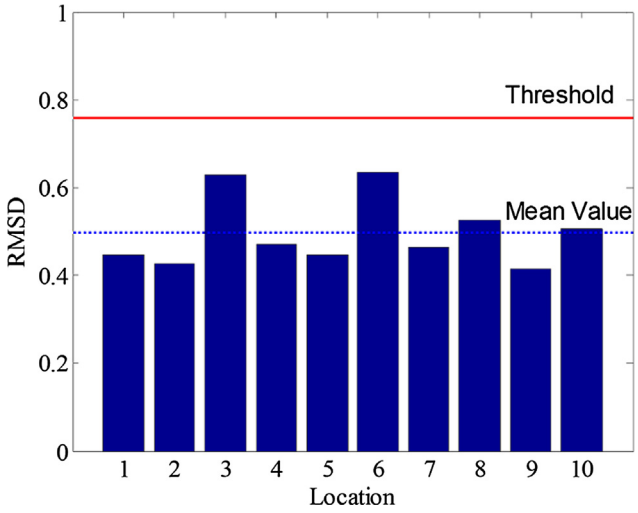

Fig. 8. The mean value (blue dotted line) and the threshold (red line). (For interpretation of the references to colour in this figure legend, the reader is referred to the web version of this article.)

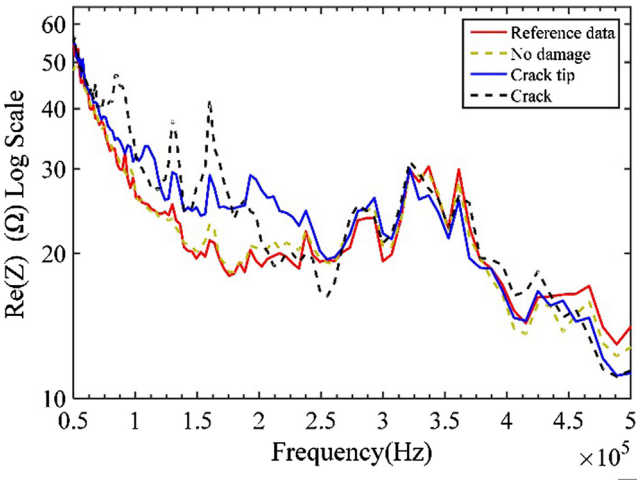

Fig. 9. Typical measured impedance signals in the local damaged area.

The proposed approach improves the efficiency of identifying the damaged area, in comparison with the EMI method, and the accuracy of characterizing the crack damage, in comparison with the Lamb wave method. Although the transducer set was only applied on a flat structure in this study, curved structures are also currently being investigated by improving the design of the mobile transducer set. Furthermore, the expansion of the scope of application of the proposed approach to real structures, such as aircraft, civil infrastructure, and heavy equipment structures, is also being explored.

The proposed approach lays a foundation for the use of intelligent mobile robot systems in damage detection. Various technologies, including intelligent path planning, sensor data fusion, and multi-agent collaboration, could be incorporated to provide the robot system with higher efficiency, increased robustness, and better performance.

Acknowledgment

This research was supported by the National Key Research and

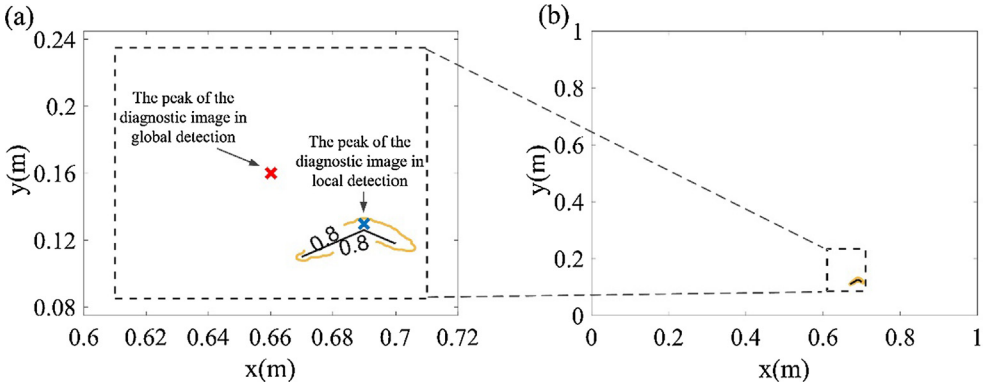

Fig. 10. Result of EMI-based local detection: (a) contour map in the local damaged area, (b) zoom out to the whole detection area. The L-shape crack is marked by a dark line, the peak of the image is marked by the blue '×', and the peak of Fig. 6 is marked by the red '×'.

Development Program of China (Grant no. 2016YFF0203002), the National Natural Science Foundation of China (Grants Nos. 11702051), the China Postdoctoral Science Foundation (Grant no. 2017M610176) and the Fundamental Research Funds for the Central Universities (DUT16ZD214).

Appendix A. Supplementary material

Supplementary data associated with this article can be found, in the online version, at https://doi.org/10.1016/j.ultras.2018.06.008.

References

[1] X.P. Qing, S.J. Beard, A. Kumar, K. Sullivan, R. Aguilar, M. Merchant, M. Taniguchi, The performance of a piezoelectric-sensor-based SHM system under a combined cryogenic temperature and vibration environment, Smart Mater. Struct. 17 (2008) 055010.
[2] C. Zhou, Z. Su, L. Cheng, Probability-based diagnostic imaging using hybrid features extracted from ultrasonic Lamb wave signals, Smart Mater. Struct. 20 (2011) 125005.
[3] Z. Su, C. Yang, N. Pan, L. Ye, L.-M. Zhou, Assessment of delamination in composite beams using shear horizontal (SH) wave mode, Compos. Sci. Technol. 67 (2007) 244–251.
[4] X. Wang, G. Foliente, Z. Su, L. Ye, Multilevel decision fusion in a distributed active sensor network for structural damage detection, Struct. Health Monit. 5 (2006) 45–58.
[5] N. Hu, Y. Cai, G. Zhu, C. Tsuji, Y. Liu, Y. Cao, Characterization of damage size in metallic plates using Lamb waves, Struct. Health Monit. 11 (2012) 125–137.
[6] C. Liang, F. Sun, C. Rogers, Coupled electro-mechanical analysis of adaptive material systems-determination of the actuator power consumption and system energy transfer, J. Intell. Mater. Syst. Struct. 5 (1994) 12–20.
[7] F. Sun, Z. Chaudhry, C. Liang, C. Rogers, Truss structure integrity identification using PZT sensor-actuator, J. Intell. Mater. Syst. Struct. 6 (1995) 134–139.
[8] Y. Yang, H. Liu, V.G.M. Annamdas, C.K. Soh, Monitoring damage propagation using PZT impedance transducers, Smart Mater. Struct. 18 (2009) 045003.
[9] C. Zuo, X. Feng, Y. Zhang, L. Lu, J. Zhou, Crack detection in pipelines using multiple electromechanical impedance sensors, Smart Mater. Struct. 26 (2017) 104004.
[10] H. Zhu, H. Luo, D. Ai, C. Wang, Mechanical impedance-based technique for steel structural corrosion damage detection, Measurement 88 (2016) 353–359.
[11] F. Zahedi, H. Huang, Time–frequency analysis of electro-mechanical impedance (EMI) signature for physics-based damage detections using piezoelectric wafer active sensor (PWAS), Smart Mater. Struct. 26 (2017) 055010.
[12] V. Giurgiutiu, Damage detection in thin plates and aerospace structures with the electro-mechanical impedance method, Struct. Health Monit. 4 (2005) 99–118.
[13] Z. Su, L. Ye, Identification of Damage Using Lamb Waves: From Fundamentals to Applications, Springer, 2009.
[14] D. Wang, L. Ye, Y. Lu, Z. Su, Probability of the presence of damage estimated from an active sensor network in a composite panel of multiple stiffeners, Compos. Sci. Technol. 69 (2009) 2054–2063.
[15] D.N. Alleyne, P. Cawley, The interaction of Lamb waves with defects, IEEE Trans. Ultrason. Ferroelectr. Freq. Control 39 (1992) 381–397.
[16] C. Valle, J.W. Littles Jr, Flaw localization using the reassigned spectrogram on laser-generated and detected Lamb modes, Ultrasonics 39 (2002) 535–542.
[17] S. Dixon, S. Palmer, Wideband low frequency generation and detection of Lamb and Rayleigh waves using electromagnetic acoustic transducers (EMATs), Ultrasonics 42 (2004) 1129–1136.
[18] S. Wang, S.L. Huang, A. Velichko, P. Wilcox, W. Zhao, A multi-objective structural optimization of an omnidirectional electromagnetic acoustic transducer, Ultrasonics 81 (2017) 23–31.
[19] P. Wilcox, M. Lowe, P. Cawley, Omnidirectional guided wave inspection of large metallic plate structures using an EMAT array, IEEE Trans. Ultrason. Ferroelectr. Freq. Control 52 (2005) 653–665.
[20] V. Giurgiutiu, A.N. Zagrai, Embedded self-sensing piezoelectric active sensors for on-line structural identification, J. Vib. Acoust. 124 (2002) 116.
[21] B. Lin, V. Giurgiutiu, Modeling and testing of PZT and PVDF piezoelectric wafer active sensors, Smart Mater. Struct. 15 (2006) 1085.
[22] Z. Wu, X.P. Qing, F.-K. Chang, Damage detection for composite laminate plates with a distributed hybrid PZT/FBG sensor network, J. Intell. Mater. Syst. Struct. 20 (2009) 1069–1077.
[23] J.-B. Ihn, F.-K. Chang, Detection and monitoring of hidden fatigue crack growth using a built-in piezoelectric sensor/actuator network: diagposics, Smart Mater. Struct. 13 (2004) 11.
[24] J.-B. Ihn, F.-K. Chang, Pitch-catch active sensing methods in structural health monitoring for aircraft structures, Struct. Health Monit. 7 (2008) 5–19.
[25] Z. Wu, K. Liu, Y. Wang, Y. Zheng, Validation and evaluation of damage identification using probability-based diagnostic imaging on a stiffened composite panel, J. Intell. Mater. Syst. Struct. 26 (2014) 2181–2195.
[26] D. Gao, Y. Wang, Z. Wu, G. Rahim, S. Bai, Design of a sensor network for structural health monitoring of a full-scale composite horizontal tail, Smart Mater. Struct. 23 (2014) 055011.
[27] V.G.M. Annamdas, Y. Yang, C.K. Soh, Influence of loading on the electromechanical admittance of piezoceramic transducers, Smart Mater. Struct. 16 (2007) 1888–1897.
[28] R.A. Wolf, Temperature dependence of the piezoelectric response in lead zirconate titanate films, J. Appl. Phys. 95 (2004) 1397.
[29] A. Raghavan, C.E. Cesnik, Effects of elevated temperature on guided-wave structural health monitoring, J. Intell. Mater. Syst. Struct. 19 (2008) 1383–1398.
[30] Q. Wang, S. Yuan, Baseline-free imaging method based on new PZT sensor arrangements, J. Intell. Mater. Syst. Struct. 20 (2009) 1663–1673.
[31] Y.-K. An, H. Sohn, Integrated impedance and guided wave based damage detection, Mech. Syst. Signal Pr. 28 (2012) 50–62.
[32] G. Park, H. Sohn, C.R. Farrar, D.J. Inman, Overview of piezoelectric impedance-based health monitoring and path forward, Shock Vib. Dig. 35 (2003) 451–463.
[33] A. Raghavan, C.E. Cesnik, Review of guided-wave structural health monitoring, Shock Vib. Dig. 39 (2007) 91–116.
[34] V. Giurgiutiu, A. Zagrai, J. Bao, Damage identification in aging aircraft structures with piezoelectric wafer active sensors, J. Intell. Mater. Syst. Struct. 15 (2004) 673–687.
[35] D. Gao, Z. Wu, L. Yang, Y. Zheng, Integrated impedance and Lamb wave–based structural health monitoring strategy for long-term cycle-loaded composite structure, Struct. Health Monit. 1475921717717312 (2017).
[36] V. Gulizzi, P. Rizzo, A. Milazzo, E. La Malfa Ribolla, An integrated structural health monitoring system based on electromechanical impedance and guided ultrasonic waves, J. Civil Struct. Health Monit. 5 (2015) 337–352.
[37] Y. Wang, Y. Zheng, D. Gao, Z. Wu, X. Qing, C. Du, Development of a new bio-inspired mobile sensing system, in: Proc. 6th European Workshop on Structural Health Monitoring, Germany, 2012.
[38] R. Gorgin, Z. Wu, Y. Zheng, A novel complementary method for the point-scan nondestructive tests based on lamb waves, Int. J. Aerosp. Eng. 2014 (2014) 1–7.
[39] W. Staszewski, C. Boller, G.R. Tomlinson, Health Monitoring of Aerospace Structures: Smart Sensor Technologies and Signal Processing, John Wiley & Sons, 2004.
[40] Z. Wang, D. Yi, X. Duan, J. Yao, D. Gu, Measurement Data Modeling and Parameter Estimation, CRC Press, 2011.